Anion vacancies as a source of persistent photoconductivity in II-VI and chalcopyrite semiconductors

Stephan Lany and Alex Zunger
National Renewable Energy Laboratory, Golden, Colorado 80401, USA
(Received 13 January 2005; revised manuscript received 12 April 2005; published 18 July 2005)

Using first-principles electronic structure calculations we identify the anion vacancies in II-VI and chalcopyrite Cu-III-VI_2 semiconductors as a class of intrinsic defects that can exhibit metastable behavior. Specifically, we predict persistent *electron* photoconductivity (n-type PPC) caused by the oxygen vacancy V_O in n-ZnO, originating from a metastable shallow donor state of V_O. In contrast, we predict persistent *hole* photoconductivity (p-type PPC) caused by the Se vacancy V_{Se} in p-$CuInSe_2$ and p-$CuGaSe_2$. We find that V_{Se} in the chalcopyrite materials is amphoteric having two "negative-U"-like transitions, i.e., a double-donor transition $\varepsilon(2+/0)$ close to the valence band and a double-acceptor transition $\varepsilon(0/2-)$ closer to the conduction band. We introduce a classification scheme that distinguishes two types of defects: type α, which have a defect-localized-state (DLS) in the band gap, and type β, which have a resonant DLS within the host bands (e.g., the conduction band for donors). In the latter case, the introduced carriers (e.g., electrons) relax to the band edge where they can occupy a perturbed-host state. Type α is nonconducting, whereas type β is conducting. We identify the *neutral* anion vacancy as type α and the doubly positively *charged* vacancy as type β. We suggest that illumination changes the charge state of the anion vacancy and leads to a crossover between α- and β-type behavior, resulting in metastability and PPC. In $CuInSe_2$, the metastable behavior of V_{Se} is carried over to the (V_{Se}-V_{Cu}) complex, which we identify as the physical origin of PPC observed experimentally. We explain previous puzzling experimental results in ZnO and $CuInSe_2$ in the light of this model.

DOI: 10.1103/PhysRevB.72.035215 PACS number(s): 71.15.Nc, 71.55.Gs, 76.30.Mi

I. INTRODUCTION

Impurities and defects in semiconductors create defect-localized states (DLS's) that are located either in the band gap, or resonate within the continuum of the host bands. In general, different host/impurity combinations may be divided into two categories: those that create localized gap states, and those that create only resonant states. For example, a DLS located within the gap and below the conduction-band minimum (CBM, "α-type behavior") is created for most 3d impurities in III-V semiconductors,[1] nitrogen,[2–4] and oxygen[3,5] in GaP, oxygen in ZnTe,[6,7] hydrogen in MgO,[8] or oxygen vacancies in Al_2O_3.[9] On the other hand, the DLS is located above the CBM ("β-type behavior") for nitrogen in GaAs,[3,4,10] oxygen in ZnS or ZnSe,[11] hydrogen in ZnO,[12] oxygen vacancies in In_2O_3,[9] as well as for all classic, hydrogenic donors in semiconductors.[13] In the "DLS-below-CBM" case, one expects a deep level that has localized wave functions and that consequently responds only weakly to external perturbations such as pressure or temperature. Even if such a defect level is occupied, it usually does not lead to conductivity due to the localized nature of the state and the ensuing high activation energy. Conversely, in the β-type situation where the DLS is resonant with the conduction band, electrons in this level will drop to the CBM, and occupy a perturbed-host state (PHS, Ref. 4) rather than the DLS. In this case, a delocalized, hydrogeniclike state is created which is conductive and responds more strongly to external perturbations, due to its host-band-like character.

There are unique cases where the *same* impurity in a solid can assume both type-α and type-β behavior. This is the case for the "*DX* center",[14] where a donor atom such as Te in AlGaAs (Ref. 15) or Cl in CdZnTe (Ref. 16) exhibits the conducting "DLS-above-CBM" β-type behavior in its normal substitutional configuration, but after a large lattice relaxation involving bond breaking,[17] it exhibits the insulating "DLS-below-CBM" α-type behavior. The hallmark of the *DX* centers is the phenomenon of persistent photoconductivity (PPC), arising from the light induced configuration change from the nonconducting ground state to the metastable conductive state.

In this paper, we discuss the interesting case where *intrinsic* defects (not impurities) exhibit both α-type and β-type behavior in the same solid, depending on their charge state. Remarkably, this occurs already for one of the simplest point defects, namely the anion vacancy in II-VI compounds and in their ternary analogs, i.e., in the I-III-VI_2 chalcopyrites. Through first-principles total-energy calculations, we show that the transition between α- and β-type configurations results in metastable behavior of these defects. Specifically, we predict that the oxygen vacancy V_O leads to persistent *electron* photoconductivity (n-type PPC) in n-ZnO observed recently after proton irradiation,[18] whereas the Se vacancy V_{Se} causes persistent *hole* photoconductivity (p-type PPC) in p-$CuInSe_2$ or p-$CuGaSe_2$, constituting the unusual case where a donorlike defect causes p-type PPC. Thus, our results shed light on hitherto unknown physical origin of the phenomenon of light-induced metastability in chalcopyrite $CuInSe_2$-based photovoltaic devices exhibiting p-type PPC.[19–23] Here, this light-induced effect can even lead to performance *enhancement*,[19,21,23] in stark contrast to "light-induced degradation" of other solar cells, e.g., Staebler-Wronski *degradation* in a-Si.[24]

 ©2005 The American Physical Society

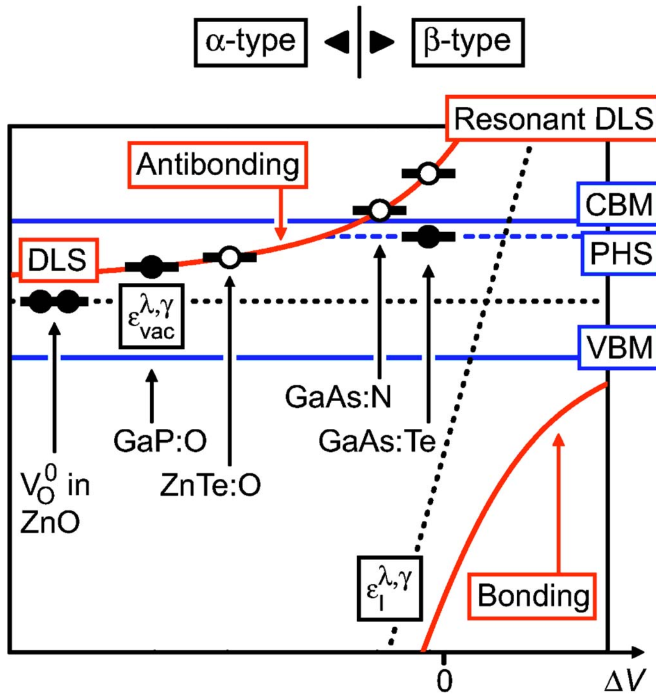

FIG. 1. (Color online) Schematic energy-level diagram of a substitutional impurity in a semiconductor. Bonding and antibonding levels (red solid lines) are formed due to the interaction between the energy level $\varepsilon_{\mathrm{vac}}^{\lambda,\gamma}$ of the pure vacancy and the atomic energy level $\varepsilon_{\mathrm{I}}^{\lambda,\gamma}$ of the impurity atom (black dotted lines), as a function of the perturbation strength $\Delta V=\varepsilon_{\mathrm{I}}^{\lambda,\gamma}-\varepsilon_{\mathrm{H}}^{\lambda,\gamma}$, where $\varepsilon_{\mathrm{H}}^{\lambda,\gamma}$ is the atomic orbital energy of the replaced host atom (λ denotes the sublattice and γ the symmetry representation). α- and β-type behavior is distinguished by the relative position of the antibonding state and the host CBM (blue solid line): The defect is α-type when the DLS is below the CBM; it is β-type when the DLS is above the CBM, and forms a PHS (blue dashed line) just below the CBM.

II. BASIC PHYSICS OF α-TYPE AND β-TYPE DEFECT BEHAVIOR

The distinction between these two types of behaviors can be appreciated from simple two-level models in which the impure system is described via the interaction between an ideal (unrelaxed) vacancy (vac) state $\varepsilon_{\mathrm{vac}}^{\lambda,\gamma}$ in the pure host crystal and the orbitals $\varepsilon_{\mathrm{I}}^{\lambda,\gamma}$ of the isolated impurity (I) atom (Fig. 1).[3,25] Here, we consider only the dilute limit, where no interaction between impurity states exists. The vacancy of the pure host crystal can occur on either sublattice λ (i.e., λ=cation or λ=anion). Different vacancy levels can be constructed from the dangling bond hybrids of the neighboring host atoms, according to the irreducible representations γ of the corresponding λ site symmetry (e.g., $\gamma=a_1$ or $\gamma=t_2$ in the T_{d} point-group symmetry of the zinc-blende structure). We define $\varepsilon_{\mathrm{vac}}^{\lambda,\gamma}$ in Fig. 1 as the energy of the λ-site vacancy state with symmetry γ. Similarly, the isolated impurity atom on site λ has symmetry-adapted orbitals with energy $\varepsilon_{\mathrm{I}}^{\lambda,\gamma}$. The two unperturbed states $\varepsilon_{\mathrm{vac}}^{\lambda,\gamma}$ and $\varepsilon_{\mathrm{I}}^{\lambda,\gamma}$ are shown in Fig. 1 as dotted lines, representing varying impurities in a fixed host system.

Vacancy and impurity states of the same symmetry γ interact and repel each other, creating bonding and antibonding states (red solid lines in Fig. 1), as a function of the perturbation strength $\Delta V=\varepsilon_{\mathrm{I}}^{\lambda,\gamma}-\varepsilon_{\mathrm{H}}^{\lambda,\gamma}$, measured by the difference of atomic orbital energies between the impurity (I) atom and the host (H) atom it replaces.[25] As one expects, for extremal values of ΔV the energy of the DLS state saturates at the value of the host vacancy level. Indeed, when one regards the vacancy itself as the impurity, the energies $\varepsilon_{\mathrm{vac}}^{\lambda,\gamma}$ of the vacancy states are not altered by interaction with an impurity state $\varepsilon_{\mathrm{I}}^{\lambda,\gamma}$. As discussed below, the energies of the vacancy states can depend strongly on atomic relaxation, however.

In order to illustrate the range of physical behaviors that is implied with the α vs β behavior, we now add in Fig. 1 schematically (for the specific case λ=anion and $\gamma=a_1$) the position of the host band edges (blue horizontal solid lines), and integrate in the figure the examples GaP:O, ZnTe:O, GaAs:N, GaAs:Te, and the neutral anion vacancy V_{O}^{0} in ZnO, which we discuss in detail below. In all those examples except for the vacancy, the occupied lower energy *bonding* state represents the impurity atomic-s state, e.g., O-2s, that lies deep below the valence-band maximum (VBM). What determines the physical behavior of the impurity is the energetic position of the DLS created by the *antibonding* combination of the vacancy and the impurity state. We see in Fig. 1 that the α-type situation is realized for strongly attractive (i.e., electronegative) impurities with $\varepsilon_{\mathrm{I}}^{\lambda,\gamma}\ll\varepsilon_{\mathrm{H}}^{\lambda,\gamma}$. The host/impurity combinations of Fig. 1 produce the following different physical properties: (i) *α-type behavior for substitution by a donor*: For example, GaP:O creates an *occupied* (closed circle in Fig. 1) deep nonconducting donor state. (ii) *α-type behavior for isoelectronic substitution*: ZnTe:O creates an *unoccupied* (open circle in Fig. 1) acceptor state in the upper part of the gap. (iii) *β-type behavior for isoelectronic substitution*: For example, GaAs:N creates an *unoccupied* resonant DLS in the conduction band, but no transition level in the band gap. (iv) *β-type behavior for substitution by a donor*: GaAs:Te creates an *occupied* shallow conducting donor state. Here, the donor electron occupies the perturbed-host state (PHS) which is created below the CBM by the long-range, screened Coulomb potential introduced by the donor substitution.

In this paper, we will show that anion vacancies in II-VI and Cu-III-VI_2 compounds can exhibit both type α and β behavior: The neutral oxygen vacancy V_{O}^{0} in ZnO shows α-type behavior, where the doubly occupied DLS is below the CBM in the band gap (Fig. 1). However, the doubly charged state V_{O}^{2+} (not shown in Fig. 1) has an unoccupied a_1^0 vacancy level above the CBM (β-type behavior with a resonant DLS), and creates a PHS below the CBM. Thus V_{O} in ZnO can assume a nonconducting configuration, where both electrons are in the deep DLS (α-type), and a conducting configuration, where the DLS is empty and the electrons occupy the shallow PHS (β-type).

Besides its use as a general classification, the distinction between scenario α and β (Fig. 1) has a technical implication on total-energy *supercell* calculations: Due to the localized nature of an α-type defect state, e.g., V_{O}^{0} in ZnO or in $\mathrm{Al_2O_3}$, the effects of impurity-impurity interaction and impurity band formation are generally weak and can be rapidly suppressed by increasing the size of the supercell.[26] However, due to the delocalized nature of a β-type defect, a highly

dispersive impurity band[4,9] forms already at rather low concentrations, leading to a Moss-Burstein shift to higher energies if the PHS is occupied. For example, Astala and Bristowe,[27] as well as Buban and co-workers[28] calculated V_O^0 in $SrTiO_3$ and observed strong changes in total energy and atomic relaxation with increasing cell size (up to 320 atoms). While long-range defect image interaction and long-range relaxation effects were invoked in Refs. 27 and 28, respectively, we note that such behavior could also be explained by the Moss-Burstein-like band-filling effect if V_O^0 in $SrTiO_3$ assumes the β-type scenario: in the limit of large supercells, the two electrons occupy the PHS, while the higher-energy DLS is unoccupied (a_1^0 configuration). With decreasing supercell size, the Moss-Burstein effect leads to an upward shift of the Fermi energy, so that the resonant DLS becomes partly occupied. Taking into account that the occupancy of the DLS controls the large lattice relaxations (viz. Ref. 29 and discussion below), both the change in total energy and in atomic relaxation can be explained by this interpretation.

III. METHOD OF CALCULATION

We use first-principles supercell calculations in order to determine the atomic structure, the single-particle defect levels, the defect formation energy ΔH, as well as thermal (equilibrium) and optical (vertical) transition energies ε for the anion vacancy in II-VI and Cu-III-Se_2 compounds. Here, the formation energy of the vacancy is defined as

$$\Delta H_{D,q}(E_F,\mu) = (E_{D,q} - E_H) + (\mu_X^{elem} + \Delta\mu_X) + q(E_V + \Delta E_F), \tag{1}$$

where $E_{D,q}$ is the total energy of the semiconductor with the defect D (here, the vacancy) in charge state q, and E_H is the energy of the pure host. The second term describes the chemical reservoir in equilibrium, where the chemical potential $\mu_X = \mu_X^{elem} + \Delta\mu_X$ of the removed anion X is given with respect to the elemental phase. For the elemental reference μ_X^{elem}, we choose the solid phase except for oxygen, where we choose the isolated O_2 molecule, i.e., $\mu_O^{elem} = \frac{1}{2}\mu_{O_2}$. The third term in Eq. (1) is the energy of the electron reservoir, i.e., the Fermi energy $E_F = E_V + \Delta E_F$ given with respect to the energy E_V of the VBM. Note that the boundaries of the allowed range of μ_X are defined by the stability condition of the host material, e.g., $\Delta\mu_{Zn} + \Delta\mu_O = \Delta H_f(ZnO)$, where ΔH_f is the calculated compound formation energy. In case of chalcopyrite, the range of chemical potentials is further restricted by formation of competing phases.[30]

The thermal transition energy $\varepsilon(q/q')$ is the Fermi energy where the lowest-energy charge state changes from q to q' as ΔE_F rises in the gap, i.e., where $\Delta H(q,E_F) = \Delta H(q',E_F)$. From Eq. (1), it follows that

$$\varepsilon(q/q') = \frac{E_D(q') - E_D(q)}{q - q'}. \tag{2}$$

We also calculate the optical (vertical) transition energies, where the following transitions are considered: (i) Excitation of electrons from an occupied defect state to the CBM; the charge state q of the defect changes by +1 during this transition. (ii) Photon emission due to the decay of an electron at the CBM into an unoccupied defect state; the charge state q changes by −1. (iii) Excitation of an electron from the VBM into the unoccupied defect state; the charge state q changes by −1. (iv) Photon emission due to the recombination of an electron in the defect state with a hole at the VBM; the charge state q changes by +1.

Keeping the VBM as reference, i.e., taking $\Delta E_F = 0$ for calculation of ΔH in Eq. (1), we calculate all optical transition energies from total energy differences. We fix the relaxed atomic positions of the initial state, assuming the Franck-Condon principle. Thus, transitions (i) and (ii) which communicate with electrons (e) at the CBM are calculated as (with $n = +1$ and $n = -1$, respectively)

$$\varepsilon_o(q/q+n;ne) = \Delta H(q+n) - \Delta H(q) + nE_g, \tag{3}$$

where E_g is the (experimental) band-gap energy. Similarly, transitions (iii) and (iv) which communicate with holes (h) at the VBM are calculated as (with $n = +1$ and $n = -1$, respectively)

$$\varepsilon_o(q/q-n;nh) = \Delta H(q-n) - \Delta H(q). \tag{4}$$

Note that only the ground-state energies for the respective charge states enter in Eqs. (3) and (4). Excitation (absorption, $n = +1$) energies are calculated as positive energies from Eqs. (3) and (4), while recombination (emission, $n = -1$) energies are calculated as negative. Such calculated optical transition energies have been used in Ref. 29 to explain the experimentally observed absorption energies in case of the color centers V_S^+ in ZnS and V_{Se}^+ ZnSe.

The total energies and atomic forces were calculated in the pseudopotential-momentum space formalism[31] within the local-density approximation (LDA) of density-functional theory. We use the Ceperley-Alder LDA exchange correlation potential as parametrized by Perdew and Zunger[32] and projector augmented wave potentials[33] as implemented in the VASP code.[34] The energy cutoff in the plane-wave expansion was up to 400 eV. Most results were obtained from supercells with 64 lattice sites for the zinc-blende and chalcopyrite structures, and with 72 sites for the wurzite ZnO, using experimental lattice constants. Brillouin-zone integrations were performed on a Γ-centered $3\times3\times3$ mesh ($3\times3\times2$ in ZnO) using the improved tetrahedron method.[35]

The well-known LDA band-gap error is corrected by acknowledging that the cation-d states in II-VI and chalcopyrites are too shallow on account of their strong, spurious self-interaction.[32(b)] Indeed, calculations in the GW approximation which largely correct for the LDA band-gap error, show, e.g., for the II-VI compounds ZnO, ZnS, and ZnSe,[36–38] and for MnO,[39] that the occupied cation-d bands shift down relative to LDA. We use here the approximate LDA+U method[40] to lower the Zn-3d (U=7 eV, J=0) and Cu-3d (U=5 eV, J=0) bands so as to yield agreement of the d-like density of states with Zn and Cu photoemission data in II-VI and chalcopyrite,[41–44] respectively. This d-band lowering weakens the p-d repulsion with the anion-p orbitals,[45] and lowers the energy of the VBM. We determine the correction ΔE_V for the energy of the VBM as the difference of the pure host VBM in LDA+U vs LDA, measured with

respect to the anion-s like Γ_{1v} state. Thus E_V in Eq. (1) is corrected by $\Delta E_V=-0.77$, -0.34 -0.28, and -0.20 eV in ZnO, ZnS, ZnSe, and ZnTe, respectively, and by $\Delta E_V=-0.37$ eV in $CuGaSe_2$ and $CuInSe_2$. The amount of correction in the VBM is consistent, e.g., with the GW calculations for ZnO.[46] Still, the LDA+U band gaps, e.g., 1.53 eV in ZnO and ~ 0 eV in $CuInSe_2$, are much smaller than the experimental gaps [3.37 eV in ZnO (Ref. 47) and 1.04 eV in $CuInSe_2$ (Ref. 48)]. The remaining discrepancy is accommodated by shifting CBM upwards (by ΔE_C). In practice, we implement this correction by using the experimental band-gap energy E_g in Eq. (3) and for the allowed range $0 \leq \Delta E_F \leq E_g$ of ΔE_F in Eq. (1). We use the LDA+U scheme only to obtain the correction for the host band edges. The formation and transition energies presented in this work are obtained from Eqs. (1)–(4) using supercell total energies that are calculated in LDA. (We find, however, that the transition energies of V_{anion} calculated from LDA+U supercell energies differ only slightly.)

In the case of β-type defects that introduce electrons in the PHS, e.g., in the case of shallow donors, a correction $n\Delta E_C$ applies to ΔH when the PHS is occupied by n electrons. This is because the donor PHS can be assumed to shift along with the host CBM during band-gap correction. Similarly, a correction $-n\Delta E_V$ is applied to shallow acceptors when the acceptor state (valence-band-like PHS) is occupied by n holes. This is because the acceptor PHS can be assumed to shift along with the host VBM during band-gap correction. In the case of α-type defects, where the electrons or holes occupy the DLS rather than the host-band-like PHS, the latter two corrections are not applied, because it cannot be assumed that the localized DLS follows the band edges during band-gap correction. This procedure of letting the shallow levels (β-type PHS) follow the host band edges, but fixing the deep levels (α-type DLS) during band-gap correction differs from our previously employed schemes of band-gap correction, e.g., in Refs. 49 and 50. Indeed, the question of the extent of LDA-correction applied to α-type levels is a significant source of uncertainty in this and other [49,50] calculations. In order to assess more quantitatively how deep, α-type levels behave upon band-gap correction, GW calculations for such deep defects will be needed.

Several further corrections to the LDA calculated energies were applied, as discussed in more detail in another publication:[51] First, Moss-Burstein-like band-filling effects (cf. Sec. II) occur when electrons or holes occupy a perturbed-host state forming an impurity band in the supercell calculation. Such band-filling effects have also to be taken into account when, e.g., an unoccupied defect level drops below the VBM in the course of atomic relaxation, thus releasing holes to the valence band (cf. Sec. V). Second, the potential alignment between a charged defect calculation and the perfect host crystal is needed in order to correct for the effect of the compensating background charge. Third, the spurious interaction of periodic image charges is corrected to $O(L^{-5})$,[52] where L is the linear supercell dimension. The present scheme of treating finite supercell size effects and LDA errors has shown to yield good results for the optical transition energies of the color center in ZnS and ZnSe,[29] when compared with experimentally observed absorption energies.

IV. ANION VACANCIES IN ZnO AND OTHER II-VI

Having introduced in Sec. II the model of α- vs β-type behavior for the general case, where the impurity atomic orbitals interact with the states of the ideal vacancy, we now turn to the levels of the relaxed anion vacancy in ZnO and other II-VI compounds. As we have shown previously,[29] the energies of the vacancy orbitals (e.g., a_1 and t_2 in T_d symmetry) depend strongly on atomic relaxation of the cation neighbors. This is because these orbitals are constructed themselves from combinations of the dangling bond hybrids centered at each of the four cation neighbors, the totally symmetric a_1 state being bonding like. An inward relaxation increases the overlap between the dangling bond hybrids, thus lowering the energy of the a_1 state. Generally, the occupation of this bonding-like state in the neutral charge state V_X^0 (a_1^2 configuration) leads to atomic relaxation that brings the neighboring cations closer, while in the ionized V_X^{2+} state (a_1^0), the cations relax outwards to a near-planar atomic configuration.[29]

A. Oxygen vacancies cause *n*-type PPC in ZnO

Figure 2(a) shows the LDA calculated angular-momentum decomposed vacancy-site local density of states (DOS) of the relaxed neutral (V_O^0) and charged (V_O^{2+}) oxygen vacancy in ZnO, and the DOS of the host semiconductor. We see that the relaxed neutral vacancy V_O^0 in ZnO [Fig. 2(a), middle panel] has an occupied a_1 symmetric (s-like) state in the band gap. [Note that the correction ΔE_V described in Sec. III shifts this level to somewhat higher energies with respect to the VBM than indicated in Fig. 2(a)] Thus V_O^0 assumes the α-type DLS-below-CBM behavior, outlined in the Introduction and in Fig. 1. The energy of this state is deepened by the *inward* relaxation of the nearest-neighbor Zn atoms towards the vacancy site, leading to a local symmetry with one Zn atom at 1.78 Å from the vacancy, and three Zn atoms at 1.83 Å from the vacancy. The resulting average Zn-Zn distance is $d_{\text{Zn-Zn}} \approx 3.0$ Å, compared to $d_{\text{Zn-Zn}} \approx 3.23$ Å in the unperturbed ZnO lattice.

When forming the ionized 2+ state V_O^{2+}, in which the DLS is unoccupied, the Zn neighbors relax instead *outwards*, leading to a configuration with a much larger $d_{\text{Zn-Zn}} \approx 4.0$ Å. As a result of the outward relaxation, the a_1 state is shifted to higher energies, becoming a broad *unoccupied* resonance in the conduction band at $\sim E_C+0.4$ eV [Fig. 2(a), bottom panel]. Thus, the ionized V_O^{2+} creates a PHS below the DLS, constituting β-type behavior.

Figure 3(a) summarizes schematically the calculated energy levels discussed above. Upon photoexcitation, the electrons in the occupied DLS of V_O^0 [Fig. 3(a), left-hand side] are promoted into the conduction band, creating the ionized state V_O^{2+} [Fig. 3(a), right-hand side]. This process is described by the semiquantitative[53] configuration coordinate diagram, shown in Fig. 3(b): First, both electrons occupy the deep and nonconducting α-type state V_O^0. The average Zn-Zn distance, serving as the reaction coordinate, is small in this configuration ($d_{\text{Zn-Zn}} \approx 3.0$ Å). Optical excitation of the V_O^0 ground state to the $V_O^+ + e$ excited state occurs at the energy $\varepsilon_o(0/+;e)=+2.83$ eV. This transition creates V_O^+ having a

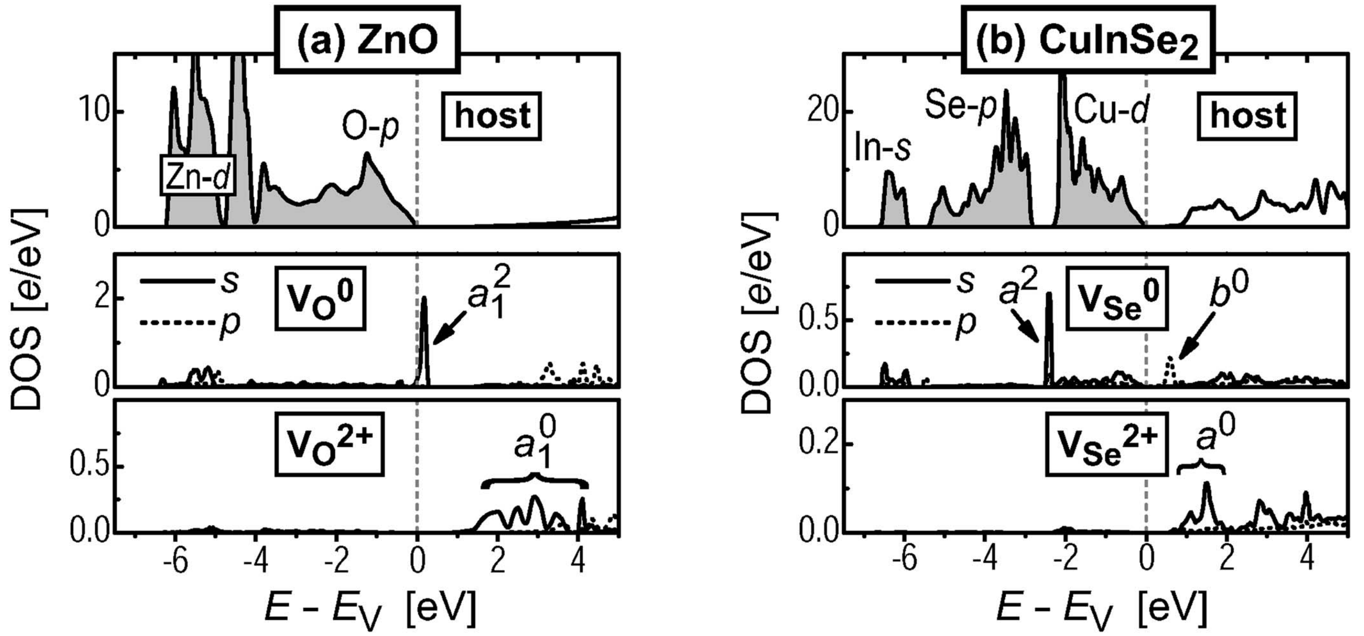

FIG. 2. Calculated density of states of the host crystals and the angular momentum decomposed local DOS at the neutral (V_X^0) and charged (V_X^{2+}) vacancy site for (a) ZnO and (b) $CuInSe_2$. The occupied DLS, i.e., the a_1^2 (V_O^0) and the a^2 (V_{Se}^0) level, and the unoccupied DLS resonance in the conduction band, i.e., the a_1^0 (V_O^{2+}) and the a^0 (V_{Se}^{2+}) level, are indicated. In $CuInSe_2$, the unoccupied b symmetry level of V_{Se}^0 is also shown.

singly occupied DLS within the band gap, i.e., being α-type. The equilibrium Zn-Zn distance of V_O^+ is estimated[53] as $d_{Zn\text{-}Zn} \approx 3.2$ Å [Fig. 3(b)]. Due to the single occupancy of the DLS, the V_O^+ state is active in electron paramagnetic resonance (EPR), and is indeed observed in EPR experiments under illumination.[54,55] A second excitation $V_O^+ \rightarrow V_O^{2+} + e$ occurs at $\varepsilon_o(+/2+;e) \approx +2.4$ eV, producing the V_O^{2+} state with $d_{Zn\text{-}Zn} = 4.0$ Å [Fig. 3(b)]. Following this large outward relaxation, the DLS moves upward, becoming resonant inside the conduction band [Fig. 3(a), right-hand side]. Consequently, the photoexcited electrons occupy the lower energy PHS rather than the DLS, i.e., the V_O^{2+} vacancy assumes β-type behavior [Fig. 3(a), right-hand side]. The electrons in the PHS are now only shallowly bound through the screened Coulomb potential.

Figure 4(a) shows as a function of the Fermi energy E_F the formation energies of the light-induced metastable configuration of V_O^0 and V_O^+ (dashed lines), relative to the corresponding formation energies in the respective equilibrium stable configuration (solid lines).[56] The transition energies in the metastable β-type configuration [open circles in Fig. 4(a)] are close to the CBM,[57] so that this configuration is conductive. These shallow binding energies of the electrons in the PHS are also schematically indicated in Fig. 3(b) by the vertical displacement of the energy curves at $d_{Zn\text{-}Zn} = 4.0$ Å. The reaction path including both excitations in Fig. 3(b) leads to the light-induced transition

$$V_O^0 \rightarrow V_O^{2+} + 2e, \tag{5}$$

which results in metastable configuration change from nonconducting α- to conducting β-behavior, constituting persistent *electron* photoconductivity (n-type PPC).

The unoccupied DLS of V_O^{2+} drops below the (experimental) CBM at a Zn-Zn distance of $d_{Zn\text{-}Zn} \approx 3.7$ Å. Since the atomic relaxation from the large Zn-Zn distance (β-type) to the small Zn-Zn distance (α-type) is controlled by the occupancy of the DLS,[29] the light-induced β-type configuration with an empty DLS (a_1^0) is (meta)stable against the depopulation of electrons from the PHS into the deep ground state with an energy barrier $\Delta E \approx 0.2$ eV [Fig. 3(b)]. In order to return into the α-type deep ground state V_O^0 with small $d_{Zn\text{-}Zn}$, the metastable state must be thermally activated across ΔE and, simultaneously, an electron must be captured by the DLS from the conduction band. The requirement of these two conditions to be met at the same time leads to a slower decay of the PPC than expected from an activation across $\Delta E \approx 0.2$ eV alone.

B. Transition and formation energies of V_O in ZnO: Comparison with experiment

We compare our calculated optical transition energies of the oxygen vacancy with recent experimental findings obtained by optically detected magnetic resonance (ODMR) (Refs. 58 and 59) and photoluminescence excitation (PLE)[60] spectroscopy studies. The green emission of ZnO around 2.45 eV was identified by ODMR as arising from a $S=1$ spin triplet state attributed to V_O.[58] In addition, the PLE experiments in Ref. 60 have shown that the $S=1$ state can be produced by sub-band-gap light of 3.1 eV. The latter energy is only little higher than our calculated optical transition energy $\varepsilon_o(0/+;e) = +2.83$ eV corresponding to the $V_O^0 \rightarrow V_O^+ + e$ transition. Thus, we interpret the experimental results in the following way: First, the neutral V_O^0 is excited to V_O^+, where the electron is released to the conduction band [the

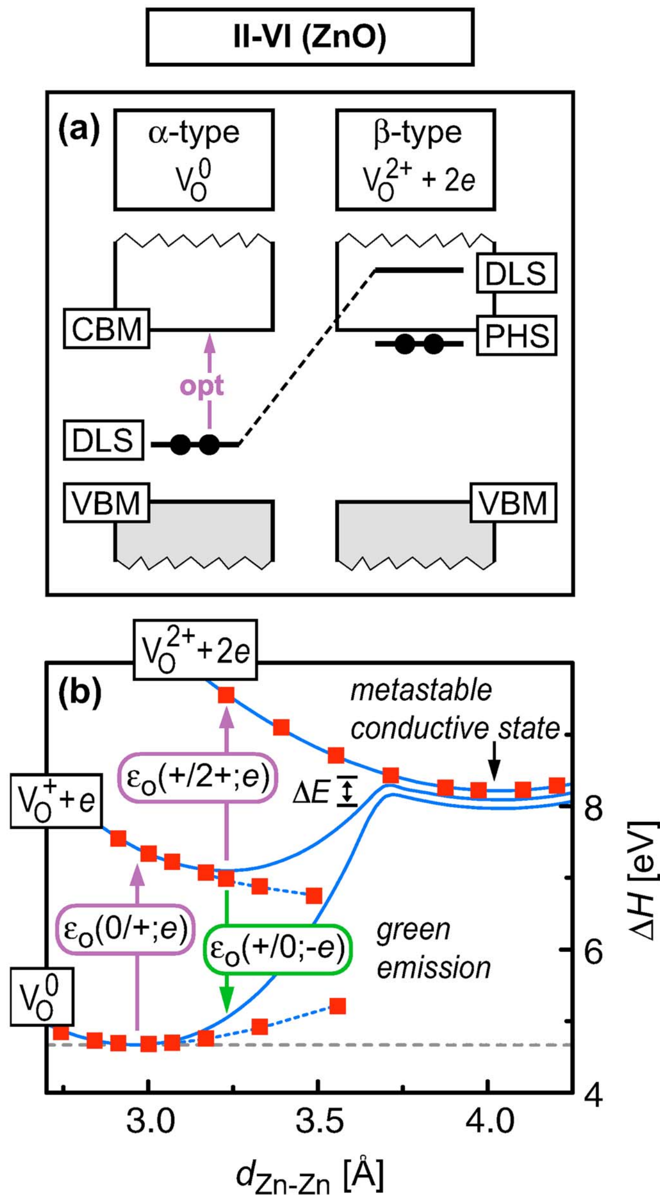

FIG. 3. (Color online) (a) Schematic energy diagram for V_O in ZnO, causing n-type PPC. Electrons that occupy the DLS or the PHS are depicted as solid circles. (b) Configuration coordinate diagram, where the calculated defect formation energies ΔH (squares) refer to oxygen-rich conditions ($\Delta\mu_O=0$). Note that the calculated formation energies $\Delta H[V_O^0]$ and $\Delta H[V_O^+]$ are underestimated when $d_{Zn\text{-}Zn}$ exceeds 3.2 Å (dotted lines, cf. Ref. 53). In these cases, the solid lines show a qualitative continuation of the ΔH. In the β-type metastable state, two electrons are released to the shallow perturbed host state, leading to n-type PPC.

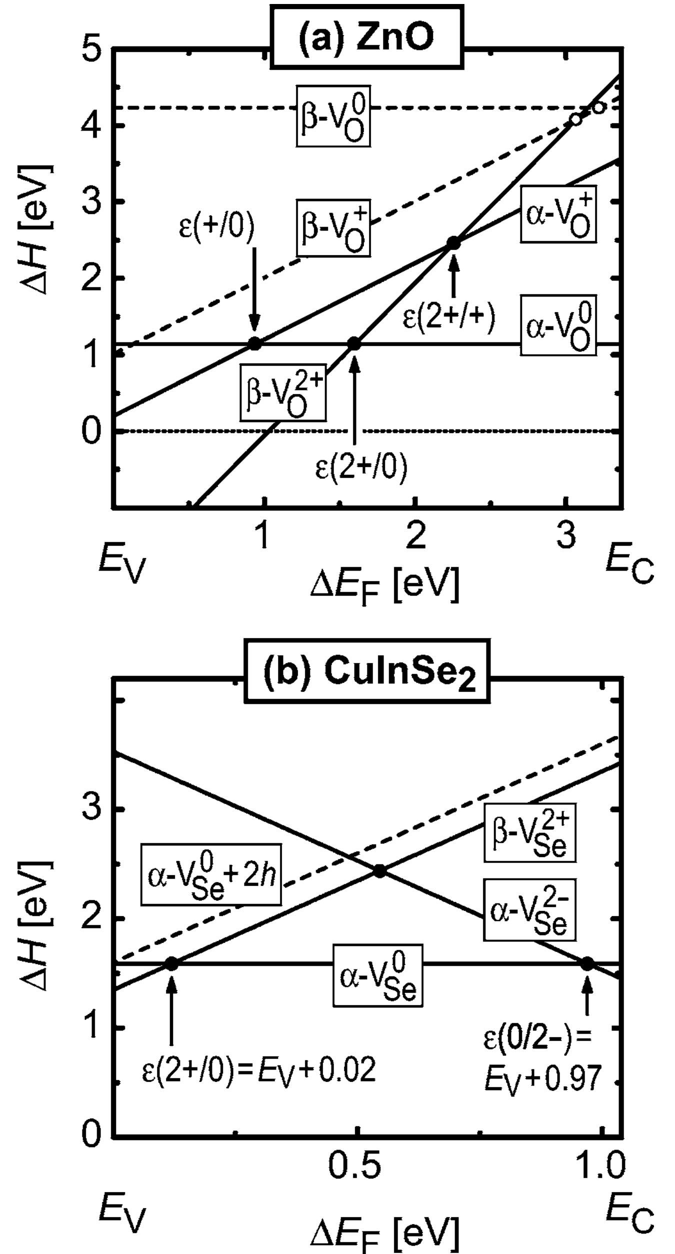

FIG. 4. Formation energies ΔH of the different charge states of V_{anion} in (a) ZnO and (b) $CuInSe_2$ in the limit of anion-poor conditions ($\Delta\mu_O=-3.53$ eV, $\Delta\mu_{Se}=-0.83$ eV), as a function of the Fermi level ΔE_F within the band gap. Solid lines and closed circles show the formation and transition energies of the equilibrium stable states, respectively.[56] Note that the line for $\Delta H(V_{Se}^{2+})$ is vertically displaced by −0.2 eV for enhanced graphical clarity. Dashed lines and open circles show the formation and transition energies in the light-induced metastable configuration. α- and β-type behavior of the respective states is indicated.

$\varepsilon_o(0/+;e)$ transition in Fig. 3(b)]. Due to its positive charge, V_O^+ creates a hydrogenic-like PHS below the CBM, which can be populated by a conduction-band electron. The spin of the electron in the PHS can align either parallel ($S=1$) or antiparallel ($S=0$) with the spin of the electron in the deep a_1^1 state (DLS) of V_O^+. While the short-lived singlet ($S=0$) state does not give rise to any ODMR signal, the triplet ($S=1$) state is active in ODMR and has a rather long lifetime, because the radiative recombination of the electron from the PHS into the DLS involves a spin flip. This recombination causes the green emission at 2.45 eV, corresponding to the theoretical $\varepsilon_o(+/0;-e)\approx -2.1$ eV transition in Fig. 3(b).[61]

The observation of a $S=1$ state in the recent experiments using moderately n-type samples contrasts with the observation of a $S=1/2$ state in the classic EPR experiments,[54,55,62] where the samples were compensated either by additional Li

doping[55] or by high-energy electron irradiation,[54,62] which creates a variety of intrinsic defects. This behavior is readily understood in our model where the α-type V_O^+ forms the triplet state by binding a conduction-band electron in n-ZnO, but not in the compensated samples, where photoexcited electrons can recombine with acceptor states, or relax from the conduction band into other donor states.

Very recently, after completion of our calculations and submission of our paper, ODMR experiments in high-energy electron irradiated ZnO were reported.[63] *Before* the electron irradiation, the $S=1$ triplet was detected, similar to what was observed in Refs. 58 and 59. This required excitation above the energy threshold of 3.1 eV required for the $V_O^0 \rightarrow V_O^+ + e$ transition. *After* the electron irradiation, only the $S=1/2$ state was observed. This state was also produced by excitation far below the 3.1 eV absorption level, indicating that in the defect-rich irradiated samples, where electrons and holes can be created by sub-bandgap illumination, there exist other channels for the excitation of the paramagnetic V_O^+ state, such as, e.g., $V_O^0 + h \rightarrow V_O^+$. In fact, already the classic F-center experiments[62] showed, in addition to the 3.1 eV level, a broad absorption band in the EPR excitation spectrum with an onset around 1.6 eV and a maximum around 2.3 eV. In Ref. 63, the authors showed that the ODMR of the $S=1/2$ state of V_O^+ results from a spin-dependent electron capture process, where an electron is transferred from a shallow donor into the a_1^1 level of V_O^+, thus forming $V_O^0(a_1^2)$. They suggest two models that cannot be distinguished by their experiment: In the first, direct model, the photoluminescence used to detect the ODMR originates from the radiative electron capture itself. Taking into account the Stokes shift, this model places the $\varepsilon(+/0)$ level at $\sim E_V + 0.9$ eV. In the second, indirect model, the luminescence results from a subsequent hole capture of V_O^0. In this model, the $\varepsilon(+/0)$ would be at $\sim E_V + 2.5$ eV. Our numerical result $\varepsilon(+/0) = 0.94$ eV is in very good agreement with the direct model (cf. Fig. 4 and discussion of thermal transition energies below), but inconsistent with the indirect model.

Whether V_O is present in ZnO in relevant concentrations, depends on the thermodynamic boundary conditions during crystal growth, i.e., on the chemical potentials $\Delta\mu$, and on the position of the Fermi energy ΔE_F in the gap, which depends on doping. For the limit of maximally oxygen-poor conditions under which $\Delta H(V_O)$ is lowest, i.e., $\Delta\mu_O = \Delta H_f(\mathrm{ZnO}) = -3.53$ eV, Fig. 4(a) shows as a function of ΔE_F the formation and transition energies for the different charge states in their equilibrium configuration (solid lines and closed circles).[64] We see that $\Delta H(V_O^{2+}) = 0$ at $E_F \approx E_V + 1$ eV, which means that V_O^{2+} forms spontaneously and acts as a hole killer when E_F approaches the VBM. The formation energy of V_O^0, being the equilibrium stable state in n-ZnO, is $\Delta H(V_O^0) = 1.14$ eV under oxygen-poor conditions, which yields an equilibrium concentration of, e.g., $c(V_O) \approx 10^{17}$ cm^{-3} at $T = 1000$ K. The rather high formation energy $\Delta H(V_O^0) = 4.67$ eV under oxygen-rich growth conditions ($\Delta\mu_O = 0$) indicates that significant concentrations of V_O would not occur under these conditions, except if E_F would be close to the VBM (i.e., in p-type ZnO), in which case ΔH of V_O is lowered by forming the ionized V_O^{2+} state [cf. Fig. 4(a)].

As a consequence of the large lattice relaxations in the neutral and in the fully ionized (2+) state, the calculated transition energies of Fig. 4(a) show a net attractive electron-electron interaction, i.e., a negative *effective* Hubbard-U of $U_{\mathrm{eff}} = -1.32$ eV, being typical for anion vacancies in II-VI semiconductors.[65] Figure 4(a) shows the thermal transition energies between the equilibrium configurations of the respective charge states (closed circles).[56] Due to the negative-U behavior, the first ionization energy $\varepsilon(+/0) = E_V + 0.94$ eV is deeper (farther from the CBM) than the second ionization energy $\varepsilon(2+/+) = E_V + 2.26$ eV, leading to a calculated $\varepsilon(2+/0)$ transition at $E_F = E_V + 1.60$ eV from the 2+ state directly into the neutral state. Owing to this deep transition level, the equilibrium stable α-type configuration of V_O^0 is not expected to provide for n-type doping. While Zn_i and hydrogen have recently been identified as a source of n-type conductivity in ZnO,[49,66,12] an additional contribution could, however, arise from PPC of V_O under illumination, due to the shallow transition energies of the β-type metastable configuration [open circles in Fig. 4(a)]. Note that the back transition from the conducting (β-type) to the nonconducting (α-type) configuration requires thermal activation across ΔE [Fig. 3(b)] and *simultaneous* capture of an electron. Thus, the lifetime of our predicted metastable shallow donor state of V_O, and hence its concentration during constant illumination, should increase with decreasing temperature and electron concentration. Our results further suggest that the recently observed[18] persistent increase of capacitance after illumination of proton-irradiated ZnO results from PPC of oxygen vacancies created by the irradiation.

Comparing our results on V_O with other first-principles calculations, we note that only the energies of the ground-state configurations [solid lines in Fig. 4(a)] have been calculated so far, and that there exists quite a spread in the values of the calculated formation and transition energies in literature. For example, $\Delta H(V_O^0)$ in the oxygen-rich regime is calculated as ~ 3 eV,[67] 4.0 eV,[68] and 5.5 eV.[49] The $\varepsilon(2+/0)$ transition energy was found within 0.5 eV from the VBM in Refs. 68 and 67, but high in the gap around $\sim E_V + 2.7$ eV in Refs. 49 and 69. Such discrepancies arise mainly due to different methodologies to correct the LDA band-gap error, but may to some extent[70] also stem from different choices of the host lattice constants, which can be taken from experiment (present work), or be determined in LDA (smaller than experiment),[68] or in the generalized gradient approximation (GGA, larger than experiment).[67] Regarding the accuracy of our present results, which are well within the range of literature data, the good agreement of the calculated optical transition energies with experimental data within our method (Ref. 29 and present work) gives us confidence that the calculated formation energies are accurate within a few tenths of an eV.

C. Anion vacancies in ZnO vs other II-VI compounds

We next discuss the possibility of metastable behavior and occurrence of PPC in other II-VI compounds. For ZnO, ZnS, ZnSe, and ZnTe, Fig. 5 shows both the calculated single-particle a_1 energy levels and the $\varepsilon(2+/0)$ transition energies

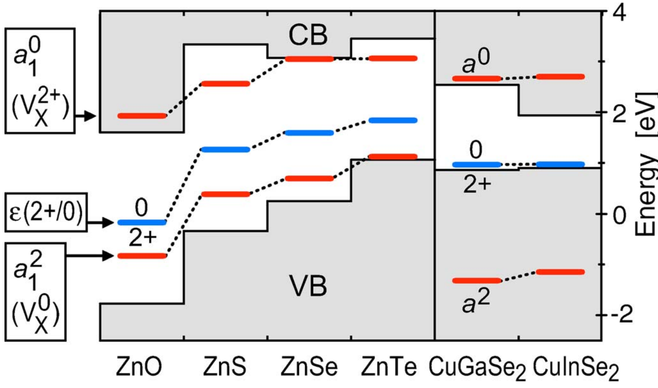

FIG. 5. (Color online) Single-particle energies of the a_1 symmetric vacancy defect levels (red) and the thermal $\varepsilon(2+/0)$ transition energy (blue) for the anion vacancy in II-VI and chalcopyrite semiconductors, relative to the host band edges. The valence-band offsets are taken from Refs. 71 and 72; the data shown take into account the correction ΔE_V (cf. Sec. III) for the position of the VBM. (The zero of the energy axis is chosen arbitrarily.)

of V_X (X=O, S, Se, and Te). The band edges are aligned according to the calculated[71,72] band offsets, taking also into account the present correction ΔE_V for the VBM (see Sec. III). According to our reaction path for the light-induced transition from α to β behavior (Fig. 3), two conditions have to be satisfied for the occurrence of PPC: (i) The neutral charge state V_X^0 must be the initial equilibrium stable state. This means that PPC can occur only when the Fermi level is above the $\varepsilon(2+/0)$ transition level. Since the calculated $\varepsilon(2+/0)$ level (blue line in Fig. 5) is located around mid-gap in all II-VI compounds, PPC can occur in n-type, but not in p-type material. (ii) V_X^{2+} must assume the conducting β-type behavior, i.e., the unoccupied a_1^0 has to be above the CBM (otherwise, the photoexcited electrons relax into the DLS and the vacancy returns into the nonconducting α-type V_X^0 state without activation). Comparing the single-particle energies of the unoccupied a_1^0 state of V_X^{2+} (red line in Fig. 5), we see that the β-type DLS-above-PHS scenario is realized only in ZnO. This reflects the unusually low conduction band (high electron affinity) of ZnO. Thus, among the Zn-based II-VI compounds, persistent photoconductivity is expected only in ZnO, provided that the Fermi level lies in the upper part of the gap above the $\varepsilon(2+/0)$ level, e.g., in n-ZnO. We note that a previous study in CdTe (Ref. 73) has shown that also the doubly charged V_{Te}^{2+} has the DLS above the CBM, so that the Te vacancy in CdTe is likely to exhibit similar metastability as V_O in ZnO.

It is interesting to compare the chemical trends in the anion vacancy electronic states along the ZnO→ZnS→ZnSe→ZnTe series while taking into account the valence-band offset.[71,72] For V_X^0, we find that the occupied a_1^2 state comes closer to the VBM along this sequence, but shifts effectively to higher energies from ZnO to ZnTe (Fig. 5). Had the Zn dangling bonds been constructed only from Zn atomic orbitals, one would expect an alignment of the Zn-Zn metal bond on an absolute scale. Analysis of the wave functions shows, however, that the dangling bonds are constructed from Zn-s/p and from anion-p orbitals of those anions that are also neighbors to the nearest-neighbor Zn atoms. Because the atomic anion-p orbital energy increases from O to Te, this admixture of O-p, S-p, Se-p, or Te-p contributions into the Zn-centered dangling bond causes an increase of the DLS energy on an absolute scale.

In ZnO, we find that V_O^0 has locally a near-tetrahedral (T_d) symmetry, with one Zn atom relaxing *inwards* by a slightly larger amount than the other three equivalent Zn neighbors. In the other II-VI compounds with larger size anions, we find an unexpected symmetry-lowering relaxation mode with orthorhombic C_{2v} symmetry,[29] where *two* cation neighbors relax *inwards* and *two* relax *outwards*. The calculated metal-metal distances around the anion vacancy are given in Table I for the different symmetries. The total-energy difference $E[C_{2v}]-E[T_d]$ between the fully relaxed and the constrained T_d symmetric structure is calculated to be −0.11, −0.32, and −0.57 eV for ZnS, ZnSe, and ZnTe, respectively,[74] showing that the lower C_{2v} is stabilized by a larger anion. This can be understood as a competition between the energy *gain* resulting from the lowering of the DLS level following by the inward relaxation, and the energy *loss* due to elastic deformation of N bonds. We see in Table I that in case of ZnO, already the near-T_d configuration with N=4 leads to a rather close Zn-Zn distance of 3.0 Å, while in the larger-anion compound ZnTe, the inward relaxation is limited by the elastic energy loss for N=4, leading to a rather large $d_{\text{Zn-Zn}}$

TABLE I. Calculated distances between the metal neighbors to the anion vacancy in II-VI and I-III-VI$_2$ semiconductors. For the dimerized (C_{2v}-like) structures, the distance between the inward (in) and outward (out) relaxing metal neighbors are given. In case of the neutral vacancy, the dimerized structure (C_{2v} like) is more stable than the symmetric (T_d-like) structure, except for ZnO. Note that the actual point-group symmetry is C_{3v} in ZnO, and C_2 in case of the chalcopyrite compounds. For comparison, the metal-metal distances in the perfect crystal are also given.

		ZnO	ZnS	ZnSe	ZnTe	CuGaSe$_2$	CuInSe$_2$
V_{anion}^0	T_d	~3.0	3.48	3.63	3.89		
V_{anion}^0	C_{2v} (in)		2.59	2.52	2.48	2.83 (Ga-Ga)	3.04 (In-In)
	(out)		4.52	4.86	5.29	4.91 (Cu-Cu)	5.15 (Cu-Cu)
V_{anion}^{2+}	T_d	~4.0	4.83	5.06	5.40	5.29 (Ga-Ga)	5.45 (In-In)
						4.96 (Cu-Cu)	5.21 (Cu-Cu)
Host		3.23	3.83	4.01	4.30	3.93	4.10

=3.89 Å. In the latter situation, energy can be further lowered by constructing the DLS from only $N=2$ dangling bond orbitals, leading to the C_{2v} symmetry and a very close Zn-Zn distance of 2.48 Å. In the ionized 2+ state, no energy can be gained from a lowering of the DLS energy (DLS is unoccupied), and the Zn neighbors relax outward to a threefold coordinated, near-planar configuration (Table I).

V. SELENIUM VACANCIES IN Cu-III-Se_2 CHALCOPYRITES

Figure 2(b) shows the angular-momentum decomposed vacancy-site local DOS of the relaxed neutral (V_{Se}^0) and charged (V_{Se}^{2+}) Se vacancy in $CuInSe_2$. We see that the relaxed V_{Se}^0 has an occupied a symmetric (s-like with respect to the V_{Se} site) state about 2 eV *below* the VBM [Fig. 2(b), middle panel]. Thus V_{Se}^0 assumes the α-type DLS-below-CBM behavior. Note that the occupied a^2 level of V_{Se}^0 in $CuInSe_2$ and $CuGaSe_2$ lies much lower in energy than the corresponding a_1^2 state of V_{Se}^0 in the same-anion material ZnSe, as shown in Fig. 5. The reason for this is the orbital structure of the relaxed nearest-neighbor cations: Whereas in II-VI semiconductors each anion has four identical cation neighbors, in chalcopyrites, e.g., $CuInSe_2$, the anion is coordinated by two Cu atoms and two In atoms. The local structure of V_{Se}^0 in $CuInSe_2$ and $CuGaSe_2$ has two cations moving inwards and two moving outwards. The total-energy calculations show that the lowest energy configuration for the anion vacancy in the chalcopyrite materials is always assumed when the dimer is formed by the group-III atoms (Ga, In) while the Cu atoms relax outward (Table I). As we found in the II-VI compounds, the wave function of the occupied DLS of V_{Se}^0 is made of s and p contributions at the cation site (Ga, In). Since the energies of the atomic cation s and p orbitals become deeper along the sequence Cu→Zn →Ga/In, this explains the very deep energies of the anion vacancy DLS in chalcopyrites (Ga-Ga dimers with deep energies) relative to II-VI compounds (Zn-Zn dimers with shallower energies). We also see why Ga-Ga and In-In dimer formation is favorable over Ga-Cu, In-Cu, or Cu-Cu combinations.

When forming the ionized 2+ state V_{Se}^{2+}, in which the DLS is unoccupied, both the neighboring Cu and group-III atoms relax *outwards* (Table I). As a result of the outward relaxation, the DLS of V_{Se}^{2+}, i.e., the a^0 single-particle level (cf. Figs. 2 and 5), is shifted to higher energies becoming an unoccupied resonance in the conduction band, similar to the situation in ZnO. Thus, we observe a change from α-(V_{Se}^0) to β-(V_{Se}^{2+}) behavior like in ZnO, but with the important distinction that the DLS of the neutral vacancy in the chalcopyrite materials is located not only below the CBM, but even *below* the VBM. These results are summarized in Fig. 6(a). In the V_{Se}^+ state where the DLS is singly occupied (a^1), the inward relaxation of the group-III atoms leads to the same structure as for V_{Se}^0 with the DLS deep below the VBM. This is seen in Fig. 6 showing schematically the calculated energy levels for V_{Se} in $CuInSe_2$ [Fig. 6(a)] and the corresponding configuration coordinate diagram [Fig. 6(b)]. During relaxation, the a^1 state of V_{Se}^+ becomes doubly occupied and releases one hole

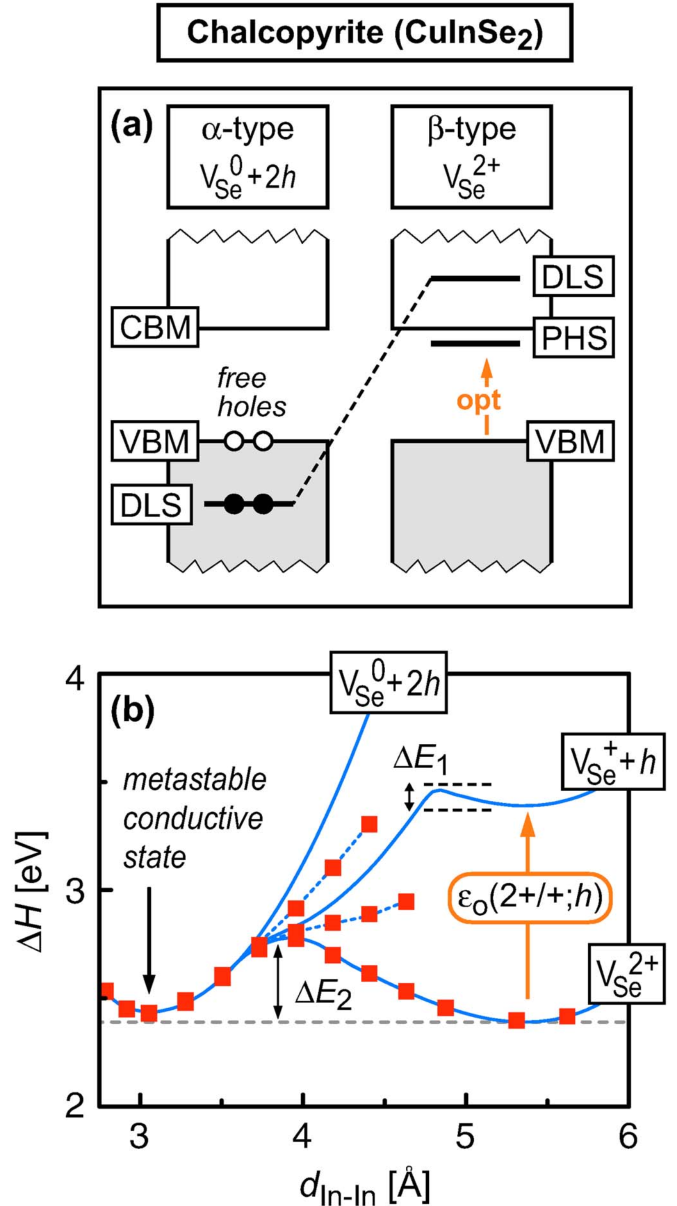

FIG. 6. (Color online) (a) Schematic energy diagram for V_{Se} in $CuInSe_2$, causing p-type PPC. (b) Configuration coordinate diagram, where the calculated defect formation energies ΔH (squares) refer to Se-rich conditions ($\Delta\mu_{Se}=0$) and to $\Delta E_F=0$ (the relative energies of the branches do not depend on ΔE_F). Note that the LDA calculated formation energies for V_{Se}^0 and V_{Se}^+ are underestimated when $d_{In\text{-}In}$ exceeds 3.9 Å (dotted lines, cf. Ref. 53). In these cases, the solid lines show a qualitative continuation of the ΔH. In the metastable α-type state, two free holes are released to the valence band, leading to p-type PPC.

to the VBM, i.e., V_{Se}^+ is unstable against $V_{Se}^+ \rightarrow V_{Se}^0 + h$. A similar behavior of V_{Se}^+ was observed in $CuGaSe_2$.[29]

Figure 2(b) shows that V_{Se}^0 introduces also an empty gap state (b^0). The p-like character in the angular momentum decomposition with respect to the vacancy site [Fig. 2(b), middle panel] indicates that this level originates from an antibonding combination of the In-centered dangling bond orbitals. When this state is occupied, V_{Se} assumes the *nega-*

tively charged states V_{Se}^{-} and V_{Se}^{2-}. While the singly charged V_{Se}^{-} and V_{Se}^{+} are unstable due to negative-U behavior, the doubly charged V_{Se}^{2-} gives rise to a very deep *acceptor* state of V_{Se} which is actually close to the CBM, i.e., $\varepsilon(0/2-)=E_V+0.97$ eV$=E_C-0.07$ eV. In $CuGaSe_2$, which has a larger band gap ($E_g=1.7$ eV), the deep acceptor level is located around mid-gap, i.e., $\varepsilon(0/2-)=E_V+1.10$ eV. Such negative, "inverted" charge states of anion vacancies have also been reported for some zinc-blende II-VI semiconductors.[75] Note, however, that the metastable effects discussed in Sec. IV and below rely only on the properties of the neutral and doubly positive states, not on the inverted negative states.

The formation energies of the stable charge states of V_{Se} in $CuInSe_2$, i.e., V_{Se}^{2+}, V_{Se}^{0}, and V_{Se}^{2-}, are shown in Fig. 4(b) as a function of ΔE_F, indicating also the respective transition energies $\varepsilon(2+/0)=E_V+0.02$ eV and $\varepsilon(0/2-)=E_V+0.97$ eV. We see that only at very low values of ΔE_F (below 0.02 eV) the system is in the V_{Se}^{2+} state, transforming directly into V_{Se}^{0} (negative-U behavior), while at E_F near the CBM, V_{Se}^{0} transforms directly into V_{Se}^{2-} (also a negative-U transition). Thus, for most of the range of ΔE_F (and actually also for realistic values of ΔE_F) V_{Se}^{0} is the ground state. The absence of any shallow donor states (contrasting with the expectation[76,77] that formation of Se vacancies is responsible for the n-type conductivity observed after Se-poor growth[78]) and the absence of any deep transitions within the experimentally accessible range of ΔE_F indicates that the *isolated* Se vacancy would hardly affect the electronic properties of $CuInSe_2$. As discussed below, however, we find that the complex formation of V_{Se} with the abundant acceptor V_{Cu} plays an important role, and gives rise to gap states and to PPC.

A. Defect physics of *p*-type PPC caused by V_{Se}

The fact that the vacancy DLS can shift to energies below the VBM in Cu-III-VI_2 compounds leads to the possibility of persistent *hole* photoconductivity (p-type PPC). While we find that the PPC actually observed in experiments is caused by the vacancy complex with V_{Cu}, the basic physics of this metastability follows already from the behavior of the isolated V_{Se}, which we discuss first: As shown in Fig. 6 the reaction pathway leading to p-type PPC in $CuInSe_2$ starts from the ionized, β-type V_{Se}^{2+} (DLS-above-PHS) state. Note that the initial *ionized* charge state V_{Se}^{2+} here is different from the initial *neutral* V_O^0 state required in ZnO. Illumination[19–23] or electron injection[79] of such $CuInSe_2$ samples create occupation of the shallow PHS [Fig. 6(a) right-hand side], The corresponding optical transition $V_{Se}^{2+}\rightarrow V_{Se}^{+}+h$, shown in the diagram of Fig. 6(b), requires an energy $\varepsilon_o(2+/+;h)$ which practically equals the band-gap energy.[80] Immediately after the optical excitation, the electron in the V_{Se}^{+} state occupies the shallow PHS rather than the DLS (viz. Fig. 6), so that the β-type configuration with the large In-In distance $d_{\text{In-In}}=5.45$ Å is stabilized. However, the DLS can capture the electron from the PHS with a small activation energy ΔE_1 [Fig. 6(b)], because the DLS energy shifts to energies below the CBM for In-In distances smaller than ~4.8 Å. After this thermally activated transition from situation β to situation α (DLS-below-CBM), atomic relaxation leads, without further activation, to the formation of the In-In dimer [$d_{\text{In-In}}=3.0$ Å, cf. Fig. 6(b), left-hand side]. During this relaxation, which is driven by the occupation of the DLS, the DLS shifts to energies below the VBM (for $d_{\text{In-In}}<3.9$ Å), and becomes doubly occupied, i.e., V_{Se}^{0} is formed. Thus the optical excitation initiates the overall reaction

$$V_{Se}^{2+} \rightarrow V_{Se}^{0} + 2h \qquad (6)$$

after which two electrons are trapped in the deep DLS [Fig. 6(a), left-hand side], and two free holes are released to the valence band, leading to p-type PPC. The energy of the metastable ($V_{Se}^{0}+2h$) state is shown in Fig. 4(b) as dashed line. Note that, in contrast to the case in ZnO, the released carriers are not bound by V_{Se}^{0} in the metastable configuration, and no new transition energies emerge as they do in ZnO [open circles in Fig. 4(a)]. However, the initial presence of V_{Se}^{2+} requires the presence of acceptors that compensate the V_{Se} double donor, and the released holes can be bound by these acceptors.

Comparing $CuInSe_2$ and $CuGaSe_2$, we see in Fig. 5 that the energy of the unoccupied a^0 level of V_{Se}^{2+} is much closer to the conduction band edge in $CuGaSe_2$. Thus we expect that electrons brought into the PHS after illumination or electron injection can be captured by the DLS practically without activation in $CuGaSe_2$ ($\Delta E_1\approx 0$). The presence of a barrier ΔE_1 in $CuInSe_2$ implies that the V_{Se}^{2+} state could be stable against capture of electrons at low temperature. Consequently, it might be possible to freeze-out the light-induced effect in $CuInSe_2$, but not in $CuGaSe_2$. However, once V_{Se}^{2+} has captured an electron, the transition into the trapped ($V_{Se}^{0}+2h$) state and the occurrence of p-type PPC should be very similar in $CuInSe_2$ and $CuGaSe_2$. In either material, the PPC is lost again when the metastable ($V_{Se}^{0}+2h$) state is thermally activated across the barrier ΔE_2 [Fig. 6(b)] towards the V_{Se}^{2+} state. Note that this process requires simultaneous capture of two holes from the valence band, so that it can be quite slow despite the moderate calculated barrier height $\Delta E_2=0.35$ Å for $CuInSe_2$.

B. Formation of (V_{Se}-V_{Cu}) vacancy complexes

Our model for the metastability of V_{Se} can account for the experimentally observed p-type PPC in $Cu(In,Ga)Se_2$. However, it requires that V_{Se}^{2+} be the equilibrium ground state, implying that the Fermi level has to be unrealistically close to the VBM, i.e., below the $\varepsilon(2+/0)=E_V+0.02$ eV transition level. Also, detailed studies[22,79] revealed that for every two electrons captured by the metastable defect, one hole trap is created. (In different words, one deep acceptor state is created for every two holes released to the valence band.) Such behavior cannot be explained by the *isolated* Se vacancy, but by a vacancy complex formed with V_{Se} and V_{Cu}, the latter being an abundant acceptor in $CuInSe_2$ and $CuGaSe_2$ due to its rather low formation energy.[81–83] We find a quite large binding energy of the vacancy complex of up to ~0.8 eV in p-type $CuInSe_2$ indicating that such complex formation plays an important role. According to the above discussion, the isolated V_{Se} is excited into the metastable state via the tran-

sition $V_{\mathrm{Se}}^{2+} \rightarrow V_{\mathrm{Se}}^{0} + 2h$. The underlying mechanism for the metastability, i.e., the formation (V_{Se}^{0}) and breakup (V_{Se}^{2+}) of In-In bonds, is still operational in the vacancy complex, leading to p-type PPC by the analogous reaction

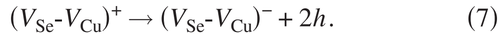

$$(V_{\mathrm{Se}}\text{-}V_{\mathrm{Cu}})^{+} \rightarrow (V_{\mathrm{Se}}\text{-}V_{\mathrm{Cu}})^{-} + 2h. \qquad (7)$$

In contrast to V_{Se}^{0}, the negatively charged vacancy complex on the right-hand side of the reaction (7) can bind one hole with the calculated activation energy $E_{\mathrm{a}}=0.27$ eV being in excellent agreement with the experimental hole trap depth 0.26 eV.[79] This energy corresponds to the $\varepsilon(0/-)$ acceptor level which is present *only* in the light-induced metastable configuration where the complex has the short-distance In-In bond. Here, the mechanism for p-type PPC requires that the positively charged complex [left-hand side of Eq. (7)] be the equilibrium ground state. The calculated $\varepsilon(+/-)=0.31$ eV transition of the vacancy complex is much deeper in the gap than the analogous $\varepsilon(2+/0)=0.02$ eV level of the isolated V_{Se}, so that the requirement of the initial $(V_{\mathrm{Se}}\text{-}V_{\mathrm{Cu}})^{+}$ state is fulfilled in p-$\mathrm{CuInSe_2}$. Therefore, we suggest that the metastability observed in actual $\mathrm{Cu(In,Ga)Se_2}$ experiments stems from the $(V_{\mathrm{Se}}\text{-}V_{\mathrm{Cu}})$ vacancy complex rather than from the isolated Se vacancy. A more detailed account of the properties of the vacancy complex will be given elsewhere.

VI. CONCLUSION

Using first-principles electronic structure calculations, we identified the anion vacancies in II-VI and chalcopyrite Cu-III-$\mathrm{VI_2}$ semiconductors as a class of intrinsic defects that can exhibit metastable behavior. The metastability arises from a crossover of the energy of the defect localized state with respect to the host band edges when the charge state is changed. Specifically, we find that the oxygen vacancy causes persistent *electron* photoconductivity (n-type PPC) in n-ZnO. Whereas in thermal equilibrium, V_{O} is deep and does not provide for n-type doping, we predict that there exists a shallow metastable state of V_{O} which could contribute to n-type conductivity under illumination. For the chalcopyrite semiconductors $\mathrm{CuInSe_2}$ and $\mathrm{CuGaSe_2}$, we find that V_{Se} causes persistent *hole* photoconductivity (p-type PPC) in p-type material, constituting the unusual case where a donor produces p-type PPC. The vacancy complex $(V_{\mathrm{Se}}\text{-}V_{\mathrm{Cu}})$ produces p-type PPC similar to the isolated Se vacancy, but, at the same time, can account for the experimental observation of a deep hole trap that appears in the metastable state. Thus, our theoretical results for the anion vacancies provide a model for the hitherto poorly understood mechanism that causes light-induced metastability in $\mathrm{CuInSe_2}$ based photovoltaic materials.

ACKNOWLEDGMENT

This work was supported by DOE EERE under Contract No. DEAC36-98-GO10337.

[1] A. Zunger, in *Solid State Physics*, edited by H. Ehrenreich and D. Turnbull (1986), Vol. 39, p. 275.

[2] D. G. Thomas, J. J. Hopfield, and C. J. Frosch, Phys. Rev. Lett. **15**, 857 (1965); D. G. Thomas and J. J. Hopfield, Phys. Rev. **150**, 680 (1966).

[3] H. P. Hjalmarson, P. Vogl, D. J. Wolford, and J. D. Dow, Phys. Rev. Lett. **44**, 810 (1980).

[4] P. R. C. Kent and A. Zunger, Phys. Rev. Lett. **86**, 2613 (2001); Phys. Rev. B **64**, 115208 (2001).

[5] D. J. Wolford, S. Modesti, and B. G. Streetman, Inst. Phys. Conf. Ser. **65**, 501 (1982).

[6] J. J. Hopfield, D. G. Thomas, and R. T. Lynch, Phys. Rev. Lett. **17**, 312 (1966).

[7] K. M. Yu, W. Walukiewicz, J. Wu, W. Shan, J. W. Beeman, M. A. Scarpulla, O. D. Dubon, and P. Becla, Phys. Rev. Lett. **91**, 246403 (2003).

[8] C. Kilic and A. Zunger, Appl. Phys. Lett. **81**, 73 (2002).

[9] I. Tanaka, K. Tatsumi, M. Nakano, H. Adachi, and F. Oba, J. Am. Ceram. Soc. **85**, 68 (2002). The authors consider only neutral vacancies and find that V_{O} in $\mathrm{Al_2O_3}$ has an occupied localized state in the gap (i.e., it is α-type), whereas V_{O} in $\mathrm{In_2O_3}$ has the localized state above the CBM and the electrons occupy a perturbed host state (i.e., it is β-type). Due to our finding of two local minima in the case of V_{O}^{0} in ZnO, we note, however, that a similar situation could be present for V_{O}^{0} in $\mathrm{In_2O_3}$, i.e., there would exist a lower-energy α-type configuration.

[10] J. D. Perkins, A. Mascarenhas, Y. Zhang, J. F. Geisz, D. J. Friedman, J. M. Olson, and S. R. Kurtz, Phys. Rev. Lett. **82**, 3312 (1999).

[11] G. W. Iseler, and A. J. Strauss, J. Lumin. **3**, 1 (1970).

[12] C. G. Van de Walle, Phys. Rev. Lett. **85**, 1012 (2000).

[13] A. K. Ramdas, Physica B & C **146**, 6 (1987).

[14] P. M. Mooney, J. Appl. Phys. **67**, R1 (1990).

[15] D. V. Lang and R. A. Logan, Phys. Rev. Lett. **39**, 635 (1977); D. V. Lang, R. A. Logan, and M. Jaros, Phys. Rev. B **19**, 1015 (1979).

[16] B. C. Burkey, R. P. Koshla, J. R. Fischer, and D. L. Losee, J. Appl. Phys. **47**, 1095 (1976).

[17] D. J. Chadi and K. J. Chang, Phys. Rev. Lett. **61**, 873 (1988); Phys. Rev. B **39**, 10063 (1989).

[18] A. Y. Polyakov, N. B. Smirnov, A. V. Govorkov, E. A. Kozhukhova, V. I. Vdovin, K. Ip, M. E. Overberg, Y. W. Heo, D. P. Norton, S. J. Pearton, J. M. Zavada, and V. A. Dravin, J. Appl. Phys. **94**, 2895 (2003).

[19] U. Rau, M. Schmitt, J. Parisi, W. Riedl, and F. Karg, Appl. Phys. Lett. **73**, 223 (1998).

[20] U. Rau and H. W. Schock, Appl. Phys. A: Mater. Sci. Process. **69**, 131 (1999).

[21] J. F. Guillemoles, L. Kronik, D. Cahen, U. Rau, A. Jasenek, and H. W. Schock, J. Phys. Chem. B **104**, 4849 (2000).

[22] J. T. Heath, J. D. Cohen, and W. N. Shafarman, J. Appl. Phys. **95**, 1000 (2004).

[23] Th. Meyer, M. Schmidt, F. Engelhardt, J. Parisi, and U. Rau, Eur. Phys. J.: Appl. Phys. **8**, 43 (1999).

[24] D. L. Staebler and C. R. Wronski, Appl. Phys. Lett. **31**, 292 (1977).
[25] H. P. Hjalmarson, Ph.D. thesis, University of Illinois, 1979.
[26] Studying V_{Se}^{0} in ZnSe for supercells containing up to 128 atoms, we found that the total energy is converged within 0.02 eV for cells with 32 atoms and larger, despite the impurity bandwidth of ~0.8 eV for the 32 atom cell. The impurity band dispersion occurs mainly close to the Brillouin-zone center, and it causes a low-energy tail of the defect state with only little density of states, hardly affecting the total energy.
[27] R. K. Astala and P. D. Bristowe, Modell. Simul. Mater. Sci. Eng. **12**, 79 (2004).
[28] J. P. Buban, H. Iddir, and S. Ögüt, Phys. Rev. B **69**, 180102(R) (2004).
[29] S. Lany and A. Zunger, Phys. Rev. Lett. **93**, 156404 (2004).
[30] Y. J. Zhao, C. Persson, S. Lany, and A. Zunger, Appl. Phys. Lett. **85**, 5860 (2004); S. Lany, Y. J. Zhao, C. Persson, and A. Zunger, *ibid.* **86**, 042109 (2005).
[31] J. Ihm, A. Zunger, and M. L. Cohen, J. Phys. C **12**, 4409 (1979).
[32] (a) D. M. Ceperley and B. J. Alder, Phys. Rev. Lett. **45**, 566 (1980); (b) J. P. Perdew and A. Zunger, Phys. Rev. B **23**, 5048 (1981).
[33] P. E. Blöchl, Phys. Rev. B **50**, 17953 (1994).
[34] G. Kresse and J. Furthmüller, Comput. Mater. Sci. **6**, 15 (1996); G. Kresse and D. Joubert, Phys. Rev. B **59**, 1758 (1999).
[35] P. E. Blöchl, O. Jepsen, and O. K. Andersen, Phys. Rev. B **49**, 16223 (1994). For atomic relaxation, we used a reduced *k*-mesh in the zinc-blende and chalcopyrite compounds, i.e., the $\left(\frac{1}{4},\frac{1}{4},\frac{1}{4}\right)$ special *k*-point. However, a calculation with the converged *k* mesh as described in the text was always performed subsequent to the relaxation.
[36] M. Rohlfing, P. Krüger, and J. Pollmann, Phys. Rev. B **57**, 6485 (1998).
[37] M. Usuda, N. Hamada, T. Kotani, and M. van Schilfgaarde, Phys. Rev. B **66**, 125101 (2002).
[38] W. Luo, S. Ismail-Beigi, M. L. Cohen, and S. G. Louie, Phys. Rev. B **66**, 195215 (2002).
[39] S. V. Faleev, M. van Schilfgaarde, and T. Kotani, Phys. Rev. Lett. **93**, 126406 (2004).
[40] A. I. Liechtenstein, V. I. Anisimov, and J. Zaanen, Phys. Rev. B **52**, R5467 (1995).
[41] C. J. Vesely, R. L. Hengehold, and D. W. Langer, Phys. Rev. B **5**, 2296 (1972).
[42] L. Ley, R. A. Pollak, F. R. McFeely, S. P. Kowalczyk, and D. A. Shirley, Phys. Rev. B **9**, 600 (1974).
[43] J. C. Rife, R. N. Dexter, P. M. Bridenbaugh, and B. W. Veal, Phys. Rev. B **16**, 4491 (1977).
[44] A. Bauknecht, U. Blieske, T. Kampschulte, J. Albert, H. Sehnert, M. Ch. Lux-Steiner, A. Klein, and W. Jaegermann, Appl. Phys. Lett. **74**, 1099 (1999).
[45] J. E. Jaffe and A. Zunger, Phys. Rev. B **29**, 1882 (1984).
[46] In Ref. 37, the authors found the VBM of ZnO lowered in the *GW* calculation by 0.49 eV with respect to LDA. However, the band-gap error and the LDA underbinding of the Zn-*d* states was not completely corrected in this *GW* calculation, so that the appropriate correction is probably somewhat larger.
[47] C. Klingshirn, Phys. Status Solidi B **71**, 547 (1975).
[48] *Copper Indium Diselenide for Photovoltaic Applications*, edited by T. J. Coutts, L. L. Kazmerski, and S. Wagner (Elsevier, Amsterdam, 1986).
[49] S. B. Zhang, S. H. Wei, and A. Zunger, Phys. Rev. B **63**, 075205 (2001).
[50] S. H. Wei, S. B. Zhang, and A. Zunger, J. Appl. Phys. **85**, 7214 (1999).
[51] C. Persson, Y. J. Zhao, S. Lany, and A. Zunger, Phys. Rev. B **72**, 035211 (2005).
[52] G. Makov and M. C. Payne, Phys. Rev. B **51**, 4014 (1995).
[53] The underestimation of the band gap in LDA implies some difficulty in constructing a fully quantitative configuration coordinate diagram for V_{O} in ZnO [Fig. 3(b)]: With increasing $d_{Zn\text{-}Zn}$, the a_1 state of the vacancy shifts to higher energies, and the transition from α- to β-behavior (DLS shifts above E_C) occurs too soon, because the CBM is at too low energy in the calculation. Thus, this transition occurs at $d_{Zn\text{-}Zn} \approx 3.2$ Å (E_C from LDA) instead of $d_{Zn\text{-}Zn} \approx 3.7$ Å (E_C from experiment). For $d_{Zn\text{-}Zn} \geqslant 3.2$ Å, this leads to an underestimation of the calculated ΔH_f in the V_{O}^{0} and V_{O}^{+} states where the a_1 level is occupied. A similar situation occurs in the case of V_{Se} in $CuInSe_2$ [Fig. 5(b)] for $d_{In\text{-}In} \geqslant 3.9$ Å.
[54] J. M. Smith and W. E. Vehse, Phys. Lett. **31A**, 147 (1970).
[55] V. Soriano and D. Galland, Phys. Status Solidi B **77**, 739 (1976).
[56] We denote here by "equilibrium stable configuration" the lower of the two energy minima of the V_{O}^{0} and V_{O}^{+} branches in Fig. 3(b) which have two local minima each. However, in a different sense, V_{O}^{+} is not equilibrium stable due to the exothermic $2V_{O}^{+} \rightarrow V_{O}^{0} + V_{O}^{2+}$ disproportion (negative-*U* behavior).
[57] The calculation of the shallow binding energies of the electrons in the extended PHS is complicated by the technical issues outlined in Sec. II. Instead, we infer from effective mass theory that both transition levels are within 0.2 eV from the CBM.
[58] F. H. Leiter, H. R. Alves, A. Hofstaetter, D. M. Hofmann, and B. K. Meyer, Phys. Status Solidi B **226**, R4 (2001).
[59] W. E. Carlos, E. R. Glaser, and D. C. Look, Physica B **308-310**, 976 (2001).
[60] F. H. Leiter, H. Alves, D. Pfisterer, N. G. Romanov, D. M. Hofmann, and B. K. Meyer, Physica B **340-342**, 201 (2003).
[61] The energy of the $V_{O}^{+}+e$ branch in Fig. 3(b) does not include the hydrogenic binding energy between the electron in the PHS and V_{O}^{+} and the energy gain due to spin alignment. These effects may reduce the emission energy somewhat.
[62] D. R. Locker and J. M. Meese, IEEE Trans. Nucl. Sci. **19**, 237 (1972).
[63] L. S. Vlasenko and G. D. Watkins, Phys. Rev. B **71**, 125210 (2005).
[64] Due to the problem described in Ref. 53, V_{O}^{+} incorrectly relaxes in LDA to the β-type "DLS-above-PHS" configuration with large Zn-Zn distance. Therefore we use here $\Delta H[V_{O}^{+}]$ corresponding to the estimated $d_{Zn\text{-}Zn}=3.2$ Å in Fig. 3(b).
[65] A. García and J. E. Northrup, Phys. Rev. Lett. **74**, 1131 (1995).
[66] D. M. Hofmann, A. Hofstaetter, F. Leiter, H. Zhou, F. Henecker, B. K. Meyer, S. B. Orlinskii, J. Schmidt, and P. G. Baranov, Phys. Rev. Lett. **88**, 045504 (2002).
[67] F. Oba, S. R. Nishitani, S. Isotani, H. Adachi, and I. Tanaka, J. Appl. Phys. **90**, 824 (2001).
[68] A. F. Kohan, G. Ceder, D. Morgan, and Chris G. Van de Walle, Phys. Rev. B **61**, 15019 (2000).
[69] C. G. van de Walle, Physica B **308-310**, 899 (2001).
[70] For example, we find that $\Delta H(V_{Se}^{0})$ in ZnSe for $\Delta\mu_{Se}=0$ (Se-rich) is lowered by ~0.28 eV when we use the LDA lattice constants instead of the experimental ones.

[71] S. H. Wei and A. Zunger, Appl. Phys. Lett. **72**, 2011 (1998).
[72] S. H. Wei and A. Zunger, J. Appl. Phys. **78**, 3846 (1995).
[73] S. Lany, H. Wolf, and Th. Wichert, Physica B **308-310**, 958 (2001).
[74] The choice of the host lattice constant affects somewhat the calculated energy differences: Using the (smaller) LDA lattice constant instead of the experimental one, we find $E[C_{2v}]-E[T_d]=+0.02$, -0.09, and -0.38 eV for ZnS, ZnSe, and ZnTe, respectively. However, using the GGA for the exchange-correlation potential and the respective (larger) GGA equilibrium lattice constant yields again a larger energy gain due to symmetry lowering and metal-metal dimer formation, e.g., $E[C_{2v}]-E[T_d]=-0.26$ eV for V_{Se} in ZnSe.
[75] D. J. Chadi, Mater. Sci. Semicond. Process. **6**, 231 (2003).
[76] S. M. Wasim, Sol. Cells **16**, 289 (1986).
[77] U. Rau and H. W. Schock, Appl. Phys. A: Mater. Sci. Process. **69**, 131 (1999).
[78] Recent theoretical studies (Ref. 30) indicate that *n*-type doping comes from In_{Cu} being the dominant donor under Se-poor conditions.
[79] M. Igalson and H. W. Schock, J. Appl. Phys. **80**, 5765 (1996).
[80] $\varepsilon_o(2+/+;h)$ may be lower than E_g by a small (<0.1 eV) amount corresponding to the shallow binding energy ($V_{Se}^{+}\rightarrow V_{Se}^{2+}+e$) of the PHS in the β-type configuration.
[81] S. B. Zhang, S. H. Wei, and A. Zunger, Phys. Rev. Lett. **78**, 4059 (1997).
[82] S. B. Zhang, S. H. Wei, A. Zunger, and H. Katayama-Yoshida, Phys. Rev. B **57**, 9642 (1998).
[83] S. H. Wei, S. B. Zhang, and A. Zunger, Appl. Phys. Lett. **72**, 3199 (1998).